Journal of Experimental Botany, Vol. 58, No. 12, pp. 3463–3473, 2007
doi:10.1093/jxb/erm203
This paper is available online free of all access charges (see http://jxb.oxfordjournals.org/open_access.html for further details)

Journal of Experimental Botany
www.jxb.oxfordjournals.org

RESEARCH PAPER

Factors contributing to accuracy in the estimation of the woody canopy leaf area density profile using 3D portable lidar imaging

Fumiki Hosoi and Kenji Omasa*

Graduate School of Agricultural and Life Sciences, The University of Tokyo, Yayoi 1-1-1, Bunkyo-ku, Tokyo, 113-8657 Japan

Received 1 May 2007; Revised 25 June 2007; Accepted 31 July 2007

Abstract

Factors that contribute to the accuracy of estimating woody canopy's leaf area density (LAD) using 3D portable lidar imaging were investigated. The 3D point cloud data for a Japanese zelkova canopy [*Zelkova serrata* (Thunberg) Makino] were collected using a portable scanning lidar from several points established on the ground and at 10 m above the ground. The LAD profiles were computed using voxel-based canopy profiling (VCP). The best LAD results [a root-mean-square error (RMSE) of 0.21 m^2 m^{-3}] for the measurement plot (corresponding to an absolute LAI error of 9.5%) were obtained by compositing the ground-level and 10 m measurements. The factors that most strongly affected estimation accuracy included the presence of non-photosynthetic tissues, distribution of leaf inclination angles, number (*N*) of incident laser beams in each region within the canopy, and $G(\theta_m)$ (the mean projection of a unit leaf area on a plane perpendicular to the direction of the laser beam at the measurement zenith angle of θ_m). The influences of non-photosynthetic tissues and leaf inclination angle on the estimates amounted to 4.2–32.7% and 7.2–94.2%, respectively. The RMSE of the LAD estimations was expressed using a function of *N* and $G(\theta_m)$.

Key words: Japanese zelkova, leaf area density (LAD), leaf area index (LAI), portable scanning lidar, three-dimensional (3D) imaging, voxel-based canopy profiling (VCP), woody canopy structure.

Introduction

The plant canopy plays important functional roles in cycling of materials and energy through photosynthesis and transpiration, maintaining plant microclimates, and providing habitats for various species (Monteith, 1973; Jones, 1992; Ehleringer and Field, 1993; Larcher, 2001; Stokes *et al*., 2006). Determining the vertical structure of the canopy is thus very important because the three-dimensional (3D) composition of the canopy helps to sustain those functional roles (Graetz, 1990; Lefsky *et al*., 2002; Schurr *et al*., 2006; Omasa *et al*., 2007). Researchers often represent the vertical foliage structure using the leaf area density (LAD) in each horizontal layer, where LAD is defined as the total one-sided leaf area per unit of layer volume (Weiss *et al*., 2004). The leaf area index (LAI), which is defined as the leaf area per unit of ground area covered by the projected area of the crown, is then calculated by vertically integrating the LAD profile data.

Although there are several ways to measure LAD and LAI, these measurements remain difficult. Stratified clipping of biomass samples is one direct measurement method. However, its application in the field is limited because of its destructive and laborious nature. Indirect methods have thus become a popular alternative. The first indirect method that was developed is the point-quadrat method, in which a probe (Warren-Wilson, 1960, 1963; Groeneveld, 1997) with a sharp point or a laser (Vanderbilt *et al*., 1990) is inserted into the canopy at a known inclination and azimuth angle, and the number of times the point contacts leaves or stems is counted. LAD and LAI can then be estimated by calculating the contact frequency,

* To whom correspondence should be addressed. E-mail: aomasa@mail.ecc.u-tokyo.ac.jp
Abbreviations: $G(\theta_m)$, the mean projection of a unit leaf area on a plane perpendicular to the direction of the laser beam at the measurement zenith angle of θ_m; LAD, leaf area density; LAI, leaf area index; lidar, light detection and ranging; *N*, number of incident laser beams in each volumetric region within the canopy; RMSE, root-mean-square error; SLA, specific leaf area; VCP, voxel-based canopy profiling.

which is defined as the mean number of contacts per insertion. However, this method is also very laborious (Norman and Campbell, 1989; Jonckheere *et al*., 2004). Another indirect method, the gap fraction method, is widely applied in field surveys and uses commercially available tools such as cameras with a fish-eye lens and optical sensors (e.g. the Li-Cor LAI-2000 Plant Canopy Analyzer; Lang and Yueqin, 1986; Neumann *et al*., 1989; Norman and Campbell, 1989; Chason *et al*., 1991; Gower and Norman, 1991; Welles and Norman, 1991; Chen and Cihlar, 1995; Eschenbach and Kappen, 1996; Welles and Cohen, 1996; Bréda, 2003; Jones *et al*., 2003). This method allows automatic estimation of LAI without destruction of the plants, and is less laborious. However, it depends on the assumption that the foliage distribution is random, which leads to errors in LAI when the foliage distribution is non-random. Although the correction factor, the so-called clumping factor, has been applied to overcome the problem (Chen and Cihlar, 1995; Leblanc *et al*., 2005), it is still a difficult problem.

Recently, lidar (light detection and ranging), which is an active remote-sensing technique that uses a laser scanner, has been applied to canopy measurements. Airborne large-footprint lidar has been used to estimate the vertical profile of the forest canopy's surface based on the waveforms of the returned pulses (Harding *et al*., 2001; Lefsky *et al*., 2002). However, the image resolution has been insufficient to provide detailed descriptions of canopy structure at the level of individual trees. Meanwhile, current airborne small-footprint lidar has made it possible to measure canopy structures with fine spatial resolution (Hyyppä and Inkinen, 1999; Omasa *et al*., 2000, 2003; Hyyppä *et al*., 2001; Brandtberg *et al*., 2003; Riaño *et al*., 2003; Holmgren and Persson, 2004; Næsset *et al*., 2004; Yu *et al*., 2004). For example, the LAI values for a Douglas-fir [*Pseudotsuga menziesii* (Mirb.) Franco] forest were estimated from the allometric relationships between tree height distribution derived from small-footprint lidar and actual LAI (Magnussen and Boudewyn, 1998). Other studies of LAI estimates using airborne lidar, in which the canopy's gap fraction was measured and converted into LAI values, were carried out for maize and sunflower (Houldcroft *et al*., 2005) and several coniferous trees (Morsdorf *et al*., 2006; Solberg *et al*., 2006). However, this work provided insufficient information about the vertical foliage structure, so the authors focused on LAI estimation rather than estimation of the vertical profile of LAD. Lovell *et al*. (2003) tried to estimate the vertical profile of LAD in eucalyptus forest using airborne small-footprint lidar, but the profile showed little response to the middle canopy levels that were present in the actual foliage profile. In this case, it seemed that the laser beams from the lidar could not reach the middle canopy due to obstruction by the upper canopy. Thus, it remains challenging to measure the LAD profile using airborne small-footprint lidar.

Portable ground-based lidar has been used to provide more accurate measurements of whole plants and vegetation canopies (Radtke and Bolstad, 2001; Omasa *et al*., 2002, 2007; Parker *et al*., 2004; Yoshimi *et al*., 2004; Hosoi *et al*., 2005; Hosoi and Omasa, 2006). Ground-based lidar is expected to compensate for the weak points of airborne lidar in LAD estimation because its fine spatial and range resolutions and its small beam size would permit measurement of the inner canopies of trees, allowing accurate estimation of LAD profiles. The optical point-quadrat method is one technique for roughly estimating LAD profiles from the ground (MacArthur and Horn, 1969). The method is based on measuring heights to the lowest leaves above a set of sample points established on the ground beneath the canopy using a telephoto lens or clinometers combined with trigonometry. LAD profiles have also been measured using portable ground-based non-scanning lidar (Radtke and Bolstad, 2001; Parker *et al*., 2004) and portable ground-based scanning lidar (Henning and Radtke, 2006). Portable ground-based scanning lidar has also been applied in the gap fraction method for the measurement of LAI (Lovell *et al*., 2003; Tanaka *et al*., 2004) and LAD profiles (Takeda *et al*., 2005). In those studies, the gap fraction within the canopy was measured using laser beams instead of sunlight. Although both methods allowed effective data collection, they provided insufficiently accurate estimates because it was difficult to illuminate the full canopy evenly. The results were also affected by non-uniformity of the actual foliage distribution and the presence of non-photosynthetic tissue.

3D imaging using portable scanning lidar has been demonstrated to provide accurate estimates of LAD (Hosoi and Omasa, 2006; Omasa *et al*., 2007). The voxel-based canopy profiling (VCP) method (in which volume elements—'voxels'—which are equivalent to the picture elements—'pixels'—in two-dimensional images) has been newly developed to improve estimates of LAD using 3D portable scanning lidar (Hosoi and Omasa, 2006; Omasa *et al*., 2007). In this method, horizontal layers of the tree canopy are fully and evenly scanned using optimally inclined laser beams emitted from several points surrounding the tree, thus solving the problem of uneven penetration of the canopy by the lidar's laser beams. From the resulting data, information about the laser traces can be expressed as voxels that serve as attributes of a 3D array. Based on the voxels, LAD profiles and the LAI of individual trees can be estimated accurately by counting the frequency of contact between laser beams and foliage of the crown in each horizontal layer. In addition, subtraction of voxel-based tree images obtained with the leafless condition from images obtained with the leafy condition allows researchers to eliminate non-photosynthetic tissues from the calculations.

However, the application has not yet been demonstrated for woody canopies. Moreover, the factors that affect the accuracy of the LAD estimation have not yet been revealed.

In the present study, 3D portable lidar imaging was applied to estimation of the LAD of woody canopy using the VCP method. The LAD estimates were first compared with actual values to validate the approach. The factors that contributed to the accuracy of the estimates were then investigated.

Materials and methods

Study site

The experiment was conducted in a mixed plantation in Ibaraki Prefecture, 40 km northeast of central Metropolitan Tokyo, Japan (35°59′N, 140°02′E). The topography was nearly flat. The dominant tree species were Japanese cedar [*Cryptomeria japonica* (L.f.) D. Don], Japanese red pine (*Pinus densiflora* Siebold & Zuccarini), ginkgo (*Ginkgo biloba* Linnaeus), and Japanese zelkova [*Zelkova serrata* (Thunberg) Makino]. The understorey included grasses, forbs, and young evergreen trees such as *Camellia japonica* Linnaeus, *Ilex integra* Thunberg, and *Ternstroemia gymnanthera* Sprague. A 4×8 m measurement plot was established at the site (Fig. 1A), and the Japanese zelkova canopy within the plot was used for the experiment (Table 1). The plot was divided into eight 2×2 m quadrats (Fig. 1B).

Direct measurement of LAD

The actual LAD of the canopy was measured directly by means of stratified clipping in September 2005. Each vertical region within each of the quadrats was divided into 16 cells (each 2×2× 0.5 m) between heights of 5 and 13 m above the ground, as shown in Fig. 1C. The entire canopy within the measurement plot was thus divided into 128 cells. Each of the cells was distinguished by a reference number of the form (l, m, n) in which (l, m) corresponds to the quadrat numbers in Fig. 1B and n is the number of the horizontal layer, with n=1 for the layer nearest to the ground (Fig. 1C). The layers below 5 m were omitted because the leaves of the Japanese zelkova canopy were distributed above this height and the understorey grew below that height. A cherry picker was brought to the study site to allow the upper region of the canopy to be reached. A laser beam was emitted vertically from the canopy to the ground using a commercially available laser pointer with a spirit level to define the corner of each quadrat for each horizontal layer within the canopy. A tape measure with a plumb bob was hung from each corner of each canopy layer to the ground to identify the height. These measures allowed identification of cells to which each leaf should be assigned.

When the positions of the leaves had been checked, they were clipped manually and labelled according to the cell they identified. Leaves corresponding to 100 g fresh weight were randomly selected from the leaves clipped from the cells located at a given height. The leaves were then scanned into JPEG images using a commercially available desktop scanner (FB636U, Canon, Inc., Japan). The relationship between the number of pixels within the images and their actual area (m^2) was determined by scanning a ruler together

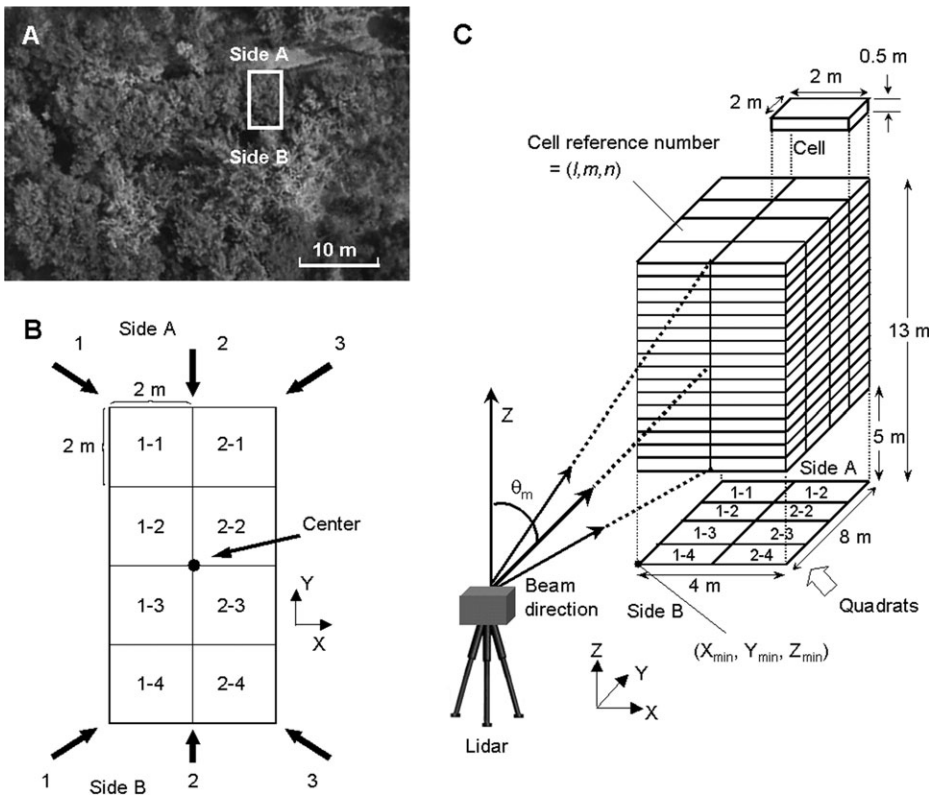

Fig. 1. The 4×8 m measurement plot established at the study site. (A) Aerial photograph of the study site. The white rectangle shows the location of the measurement plot that includes a Japanese zelkova canopy [*Zelkova serrata* (Thunberg) Makino]. (B) Quadrats established on the ground in the measurement plot. Each quadrat is 2×2 m. The black dot shows the centre of the measurement plot. Black arrows show the directions in which lidar scanning was performed. (C) Illustration of the cells established within the measurement plot from 5 m above the ground to a height of 13 m. In total, 128 cells (each 2×2× 0.5 m) were measured. θ_m represents the measurement zenith angle.

Table 1. *Descriptive variables for the Japanese zelkova canopy [*Zelkova serrata *(Thunberg) Makino] within the measurement plot at the study site*

Tree name	Height (m)	LAI (m^2 m^{-2})	LAD (m^2 m^{-3})		Specific leaf area (m^2 kg^{-1})	
			Mean	Maximum	Mean	SD[a]
Zelkova serrata (Thunberg) Makino	12.5	4.59	0.57	1.51	11.9	2.5

[a] SD, Standard deviation.

with the leaves. The number of pixels of leaves within the images was then converted into the actual leaf area by multiplying the number of leaf pixels by the area per pixel. After scanning, the leaves were dried to constant weight in an oven at 80°C, and the dry weight was measured. The actual leaf area and corresponding dry weight of the oven-dried samples were converted into an area to dry weight ratio (i.e. specific leaf area, SLA) at each height. It was observed that SLA decreased as height increased. All other leaves were also dried under the same conditions so that the total dry weight could be measured for each cell. Leaf area in each cell was determined by multiplying the dry weight in a cell by the SLA corresponding to the height of the cell. Consequently, LAD in each cell was acquired by dividing the leaf area by the cell volume (2 m^3). By integrating the LAD values vertically, actual values of LAI could be obtained for each quadrat and for the whole canopy.

Measurements using two types of portable scanning lidar

A portable fine-resolution scanning lidar that calculates distances based on trigonometry (a modified TDS-130L 3D laser scanner; Pulstec Industrial Co., Ltd, Japan) was used to measure leaf inclination angle. The lidar's measurable range is 3.5–10 m. The range and scan resolutions are about 1 mm and 2 mm, respectively, at a measurement range of about 5 m. A rotating mount with a stepper motor and a galvano mirror within the lidar head automated the horizontal and vertical scanning. Leaves within quadrats 1-1 and 2-1 (see Fig. 1B) were scanned by the lidar from a position on side A, about 5 m from the centre of the measurement plot, in August 2005. Each leaf was distinguishable from the acquired 3D point cloud image of the leaves because of the fine resolution. After randomly selecting 200 leaves in the image, each leaf was approximated as a plane, and normals to the planes were estimated. The distribution of leaf inclination angles was derived from the angles of these normals with respect to the zenith.

Another type of portable scanning lidar (LPM-25HA, RIEGL, Austria) was used for the application of the VCP method. The portable lidar was able to obtain the distance to the surface of an object between 2 m and 60 m from the sensor by measuring the time elapsed between the emitted and returned laser pulses (the 'time of flight' method). A rotating mount driven by built-in stepper motors with 0.009° accuracy panned and tilted the lidar head. The lidar had an accuracy of ±8 mm when computing the range of each sample point. The Japanese zelkova canopy within the measurement plot was scanned by the lidar from several ground positions (positions 1, 2, and 3 on sides A and B; Fig. 1B) in August 2005. The centre of the angles of the laser beams from the zenith (= the measurement zenith angle, θ_m; Fig. 1C) was 47.2, 57.8, and 71.3° at each measurement position except the case of 71.3° at B2, where the measurement position could not be set because of the presence of a dense understorey in that position.

The distance between the canopy and the lidar position was adjusted as laser beams at each measurement zenith angle hit the region of the canopy at heights between 8 m and 13 m, where leaves grew most densely, and the scan zenith angle of the laser beam (i.e. the range of angles on either side of the central zenith angle within the vertical plane) was chosen so that the laser beam could cover the canopy from 5 m to 13 m in height. The average distances from the centre of the measurement plot (Fig. 1B) at the measurement zenith angles of 47.2, 57.8, and 71.3° were 9.3, 13.6, and 24.4 m, respectively. The scan zenith angles to the measurement zenith angles of 47.2, 57.8, and 71.3° were ±19.1, ±10.0, and ±10.6°, respectively. The scan azimuth angle (the range of angles on either side of the central zenith angle within horizontal plane) ranged from ±14° to ±47° so that the laser beams could cover the entire width of the canopy. The increments of the azimuth and zenith angles were set at 0.054° for the three measurement zenith angles.

The canopy was also measured from positions 10 m above the ground using the cherry picker. Because there were few places at the study site where the cherry picker could be installed, measurements were carried out from only three positions at this height, corresponding to position 2 on side A and positions 1 and 3 on side B. The measurement zenith angle of the laser beams was 90.0° (i.e. horizontal direction) and the corresponding scan zenith angle at this height was ±33.1°. The azimuth scan angle ranged from ±18° to ±28°. The increments of the azimuth and zenith angles were set at 0.054°. The average distance between the three lidar positions 10 m above the ground and a point 10 m above the centre of the measurement plot was 12.8 m. After the measurements during the leafy condition in August 2005, the same canopy was measured from the ground in February 2006, during the leafless condition. The measurement conditions used at this time were the same as those used for the 57.8° measurement zenith angle during the leafy condition.

Voxel-based computation of LAD

LAD computation used the VCP method (Hosoi and Omasa, 2006). The complete data set for each measurement zenith angle was typically composed of point cloud data obtained from each of the six measurement positions, but only five data sets were obtained at the measurement zenith angle of 71.3° and only three were obtained at the 10 m height. The individual coordinate systems for these data were registered into a single point-cloud data set with a common 3D coordinate system for each measurement zenith angle using the iterative closest-point algorithm (Besl and McKay, 1992). The data measured in the leafless condition were also registered using this algorithm. All points in the registered data set were converted into voxel coordinates for each measurement zenith angle using the following equations:

$$i = Int\left(\frac{X - X_{\min}}{\Delta i}\right) + 1 \quad (1)$$

$$j = Int\left(\frac{Y - Y_{\min}}{\Delta j}\right) + 1 \quad (2)$$

$$k = Int\left(\frac{Z - Z_{\min}}{\Delta k}\right) + 1 \quad (3)$$

where (i, j, k) represent the voxel's coordinates within the voxel array, *Int* is a function that rounds off the result of the calculation to

the nearest integer, (X, Y, Z) represent the point coordinates of the registered lidar data, (X_{min}, Y_{min}, Z_{min}) represent the minimum values of (X, Y, Z) (Fig. 1C), and (Δi, Δj, Δk) represent the voxel element size. In this experiment, the voxel element size, which depended on the range and scan resolution of the lidar, was 5×5×5 mm. Non-photosynthetic tissues such as trunks and branches and understorey were excluded by extracting the corresponding points between the 3D voxel data in the leafless condition and the one in the leafy condition.

To apply the VCP method, voxels corresponding to coordinates converted from points within the registered data set were assigned an attribute of 1 (Hosoi and Omasa, 2006). A voxel with an attribute of 1 represents a voxel in which at least one laser beam was intercepted by leaves. All laser beams emitted from the lidar positions were then traced within the voxel array in accordance with the actual laser beam angles. If voxels that did not have an attribute of 1 were intersected by at least one laser beam trace, the voxel was assigned an attribute of 2. A voxel with an attribute of 2 therefore represented a voxel through which one or more laser beams passed without touching a leaf. Other voxels that were assigned neither attribute value were omitted from the LAD computation. Based on the attribute values, LAD was computed in each of the cells within the measurement plot using the following equation:

$$\mathrm{LAD}_{lmn} = \frac{\cos\theta_{lmn}}{G(\theta_{lmn})} \cdot \frac{1}{\Delta H} \sum_{k=m_h}^{m_{h+\Delta H}} \frac{n_I(k)}{n_I(k) + n_P(k)}. \quad (4)$$

where (l, m, n) represent the cell reference number, θ_{lmn} is the mean zenith angle for all laser beam incidences within a cell, and $n_I(k)$ and $n_P(k)$ are the numbers of voxels with attributes of 1 and 2 in the kth layer of a cell, respectively. Thus, $n_I(k)+n_P(k)$ represents the total number of incident laser beams that reach the kth layer of a cell. $G(\theta_{lmn})$ is the mean projection of a unit leaf area on a plane perpendicular to the direction of the laser beam at θ_{lmn} (Norman and Campbell, 1989; Welles and Norman, 1991; Jonckheere *et al*., 2004; Weiss *et al*., 2004). The term $\cos(\theta_{lmn})[G(\theta_{lmn})]^{-1}$ is a correction factor for the influence of leaf inclination angle and laser beam direction. ΔH is the vertical thickness of a cell (=0.5 m), and m_h and $m_{h+\Delta H}$ are the voxel coordinates on the vertical axis and are equivalent to the height of the bottom of cell h and the top $h+\Delta H$ in orthogonal coordinates ($h=m_h\,\Delta k$). Equation (4) is analogous to the equation of radiation transfer through canopy in the case of neglecting the scattering term (Ross, 1981; Anisimov and Fukshansky, 1993). $n_I(k)+n_P(k)$ and $n_I(k)$ in Equation (4) correspond to the radiation intensity and the attenuation of the radiation intensity in the radiation transfer equation. $\cos(\theta_{lmn})[G(\theta_{lmn})]^{-1}$ was determined following the method of Hosoi and Omasa (2006) using the distribution of leaf inclination angles acquired by the fine-resolution portable lidar, as described above. A constant value of 1.1 was chosen for $\cos(\theta_{lmn})[G(\theta_{lmn})]^{-1}$ for the measurement zenith angle of 57.8°, which is near the particular angle of 57.5° at which the value can be considered nearly independent of leaf inclination (Warren-Wilson, 1960; Weiss *et al*., 2004).

From the LAD estimates computed for each of the cells, the LAD profile in each quadrat was obtained for each measurement zenith angle. By vertically integrating the LAD estimates within the same quadrat, an LAI estimate for each quadrat was obtained. By averaging the LAD profiles horizontally, the LAD profile in the measurement plot (eight quadrats) was also obtained. The vertical integration offered an LAI estimate for the measurement plot. The influence of non-photosynthetic tissues on the results in the measurement plot was assessed for each measurement angle by comparing LAD estimates with and without these tissues. When the distribution of leaf inclination angle cannot be obtained and then the influence of leaf inclination is not corrected, it causes an estimation error except at a laser zenith angle around 57.5°. The error at each measurement zenith angle was assessed from the mean value of $\cos(\theta_{lmn})[G(\theta_{lmn})]^{-1}$ for all cells in the measurement plot.

Derivation of the relationship between the error of LAD estimation and the number of incident laser beams

The relationship between the number of incident laser beams in each cell (N) and the error of the LAD estimates was also investigated. Laser beams were traced again as described above for the voxel-based computation of LAD, and N was calculated by counting the number of laser beam traces that passed through each cell. Each cell was then sorted into classes based on N. The root-mean-square error (RMSE) of the LAD estimates in each class was calculated from the errors of the LAD estimates for the cells included in each class. This enabled the establishment of a relationship between the RMSE of the LAD estimates and N. These relationships were derived and compared for all measurement zenith angles. After this comparison was complete, the value of $G(\theta_m)$ for each of the angles was calculated and the RMSE at each angle was expressed as a common function of N and $G(\theta_m)$.

Results

Figure 2 shows 3D lidar images of the zelkova canopy after registration of the images measured at a measurement zenith angle of 57.8° from the six ground positions indicated in Fig. 1. Trees in the measurement plot were extracted as shown in Fig. 2B(a) from the overall image shown in Fig. 2A, and then the non-photosynthetic tissues, including undergrowth (Fig. 2Bb), and the photosynthetic tissues (Fig. 2Bc) were separated. Each tissue was clearly distinguishable because of the fine resolution of the images. The percentages of non-photosynthetic tissue area to total surface area at heights above 5 m were 4.2, 15.7, 32.7, and 4.4% for the measurement angles of 47.2, 57.8, 71.3, and 90.0°, respectively, based on the estimates derived from the lidar data. These non-photosynthetic tissues cause errors in the estimation of LAD.

Figure 3 shows the distribution of leaf inclination angles within the zelkova canopy in the measurement plot in Fig. 1B using the fine-resolution portable scanning lidar. The values ranged from 0° to 65°, with a mean value of 18.6°, as most angles were less than about 30°. The distribution of leaf inclination angles allowed calculation of the values of $\cos(\theta_{lmn})[G(\theta_{lmn})]^{-1}$ in each cell. The mean values of $\cos(\theta_{lmn})[G(\theta_{lmn})]^{-1}$ for all cells at measurement angles of 47.2, 71.3, and 90.0° were 1.08, 0.90, and 0.80, respectively. With no correction for leaf inclination, the errors in LAD estimation were estimated as 7.2, 14.2, and 94.2% on average for all cells at measurement angles of 47.2, 71.3, and 90.0°, respectively. The results showed the significant level of the error at the measurement angle of 90.0°. The value of $\cos(\theta_{lmn})[G(\theta_{lmn})]^{-1}$ at around 90.0° changes very sensitively according to the leaf inclination and laser zenith angle when the distribution of leaf inclination angle is planophile as is in the present study.

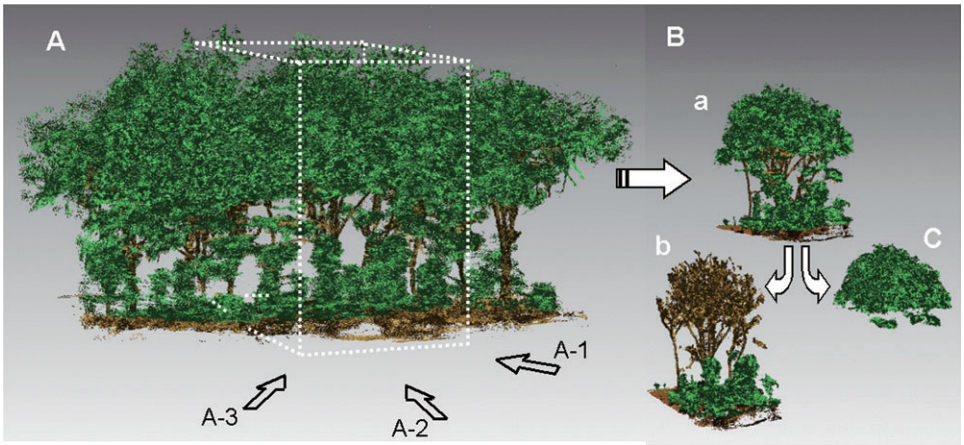

Fig. 2. 3D images of the Japanese zelkova canopy at the study site. This image shows the results after co-registration of the images measured at a measurement zenith angle of 57.8° from the six positions on the ground shown in Fig. 1B. Leaves are coloured green and the other plant parts are coloured brown. (A) A section of the Japanese zelkova canopy at the study site. The area enclosed by the white broken line corresponds to the measurement plot. Arrows show the directions of lidar scanning from side A. (B) Separation of the image into its components: (a) Trees in the measurement plot. (b) Separation of non-photosynthetic tissues, including undergrowth. (c) Separation of photosynthetic tissues (i.e. foliage).

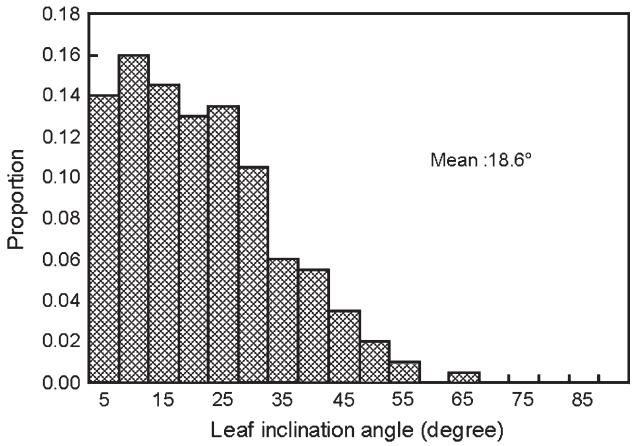

Fig. 3. Distribution of leaf inclination angles in the Japanese zelkova canopy derived from a high-resolution portable scanning lidar image. Mean=the mean leaf inclination angle.

Thus, the correction based on the actual leaf inclination angle is particularly essential for the measurement angle around 90.0°. Although a constant value of 1.1 was applied for $\cos(\theta_{lmn})[G(\theta_{lmn})]^{-1}$ at a measurement angle of 57.8°, the validity of this assumption was tested using the actual distribution of leaf inclination angles and the actual zenith angles of the laser beams for each cell. The resulting values ranged from 1.04 to 1.06, depending on the cell. The difference between the assumed value of 1.1 and the values derived from actual data was <5.5%, and the choice of a constant value was thus reasonable for a measurement angle of 57.8°.

The LAD profiles estimated by eliminating non-photosynthetic tissues from the lidar data were compared with the actual stratified clipping values for an entire region within the measurement plot (Fig. 4). All LAD estimates agreed well with the actual values up to a height of 8.5 m. However, the estimates at measurement angles of 47.2–71.3° underestimated the actual values above this height. The estimate at 90.0° also underestimated the actual value at heights above 10.0 m, but the degree of underestimation was less than at the other angles. RMSE values for all estimates in the LAD profiles were 0.33, 0.40, 0.55, and 0.24 $m^2\ m^{-3}$ at measurement zenith angles of 47.2, 57.8, 71.3, and 90.0°, respectively. The LAD estimates showed that smaller zenith angles had lower RMSE values, but that the 90.0° angle produced the lowest RMSE. The mean values of N for all cells at measurement angles of 47.2, 57.8, 71.3, and 90.0° were 5.3×10^4, 2.5×10^4, 2.0×10^4, and 1.3×10^4 incidences m^{-3}, respectively. The LAD estimates also showed that RMSE decreased with increasing N, except at the 90.0° angle. The absolute errors in LAI for the measurement plot were 23, 37, 57, and 4.1% at measurement zenith angles of 47.2, 57.8, 71.3, and 90.0°, respectively.

It seemed to be a problem that the largest discrepancies between the actual and the estimated LAD profiles for an entire region within the measurement plot (Fig. 4) occurred in the top layer, because most light interception, energy, and mass exchanges occur in the top layers of the canopy. However, in the LAD estimation of each quadrat, good agreements between the actual values and estimates up to the top layers were obtained in some quadrats. To provide examples of the LAD profiles for each quadrat, the estimated LADs in quadrats 1-1 and 2-3 were compared with the actual values (Fig. 5). The estimates for quadrat 1-1 (Fig. 5A), which was close to the lidar position on side A, showed good agreement with the actual values at all measurement zenith angles. However, the LAD estimates at quadrat 2-3 were overestimates of the actual values at heights of about 7–9 m, but

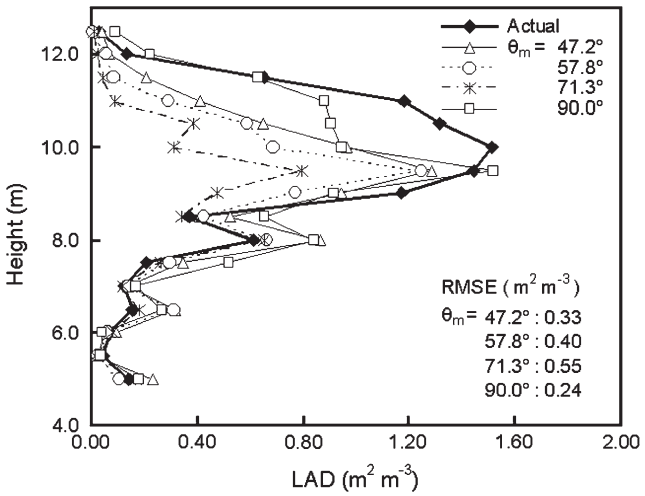

Fig. 4. Comparison of LAD profiles for the measurement plot between the lidar-derived estimates obtained with different measurement zenith angles (θ_m) and the actual value. RMSE, root-mean-square error of the LAD estimates.

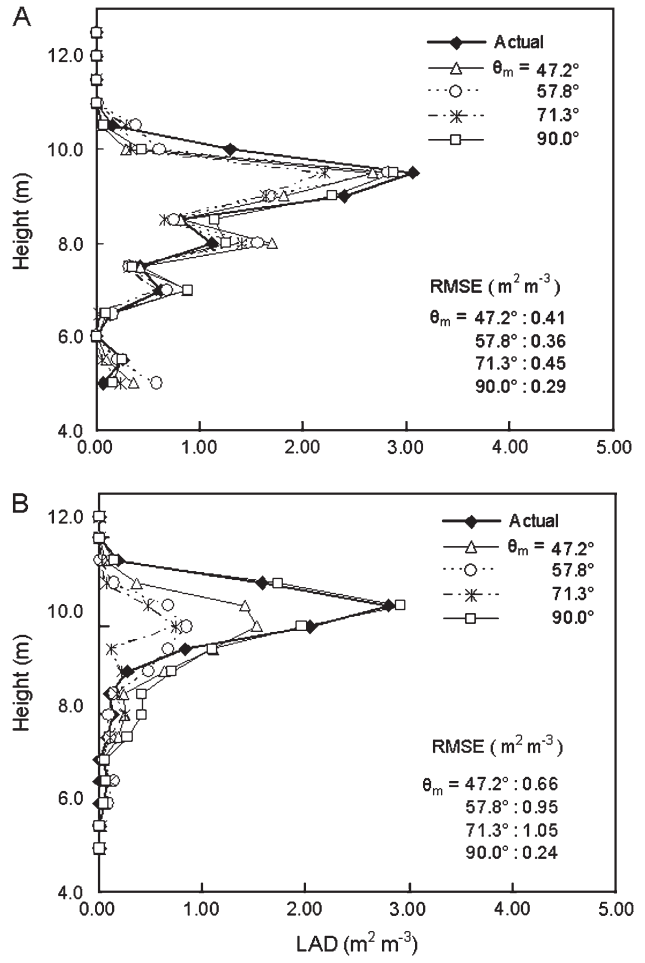

Fig. 5. Comparison of LAD profiles in two quadrats between the lidar-derived estimates obtained with different measurement zenith angles (θ_m) and the actual value. (A) Quadrat 1-1. (B) Quadrat 2-3. RMSE, root-mean-square error of the LAD estimates.

underestimated the actual values at greater heights, except at a measurement angle of 90.0° (Fig. 5B); this quadrat was in the middle of the measurement plot. The same tendency was observed in the other quadrats, i.e. the closer the quadrats were to the lidar positions, the smaller the underestimation of the actual LAD value, except at the 90.0° measurement angle. Compared with the LAD estimates at other angles, the estimates at 90.0° offered less underestimation for quadrats near the middle, but showed slight overestimation at heights of <10.0 m. The mean RMSEs of the LAD estimates for each quadrat were 0.50, 0.64, 0.78, and 0.44 $m^2\ m^{-3}$ at measurement zenith angles of 47.2, 57.8, 71.3, and 90.0°, respectively. The mean absolute errors of LAI for each quadrat were 21, 37, 57, and 12.7% at angles of 47.2, 57.8, 71.3, and 90.0°, respectively.

To improve the error of the LAD estimates, the underestimated values at a measurement angle of 57.8° were replaced with the estimates derived from the measurements at a height of 10 m (θ_m=90.0°). Figure 6 shows the results for the entire region within the measurement plot (Fig. 6A) and for quadrat 2-3 (Fig. 6B). The measurement zenith angle of 57.8° was chosen to represent the ground measurements because of the usefulness of the leaf inclination correction in the field and the fact that the accuracy at this angle was comparable with the best accuracy (at an angle of 47.2°). The RMSEs were decreased from 0.40 $m^2\ m^{-3}$ to 0.21 $m^2\ m^{-3}$ for the entire region within the measurement plot and from 0.95 $m^2\ m^{-3}$ to 0.12 $m^2\ m^{-3}$ for quadrat 2-3. The mean RMSE of the LAD estimates for each quadrat improved from 0.64 $m^2\ m^{-3}$ to 0.36 $m^2\ m^{-3}$. The errors of LAI also improved, from 37% to 9.5% for the absolute error for the entire region and from 37% to 9.6% for the mean for each quadrat.

Figure 7 shows the relationship between RMSE of the LAD estimates and N in each cell for the measurement zenith angles of 47.2° (Fig. 7A), 57.8° (Fig. 7B), 71.3° (Fig. 7C), and 90.0° (Fig. 7D). The slope of the regression lines increases as the measurement zenith angle increases, so large measurement angles offer more accurate estimates than small angles when the value of N exceeds a certain value (e.g. $N > 0.3\times10^4$ incidences m^{-3} for 90.0°, estimated from the intersection points of the regression lines in Fig. 7A–D). In particular, the rate of decrease of RMSE with increasing N is higher at the 90.0° angle than at the other angles, so that better LAD estimates (as shown in Figs 4 and 5) have been obtained even though the mean value of N for all cells at this angle ($= 1.3\times10^4$ incidences m^{-3}) was the smallest of all the angles. Although the 71.3° angle offered the worst result (Fig. 4), Fig. 7C suggests that this angle offers better results than the 47.2° and 57.8° angles when a sufficient number of laser beam incidences is supplied ($N > 3.2\times10^4$ incidences m^{-3}).

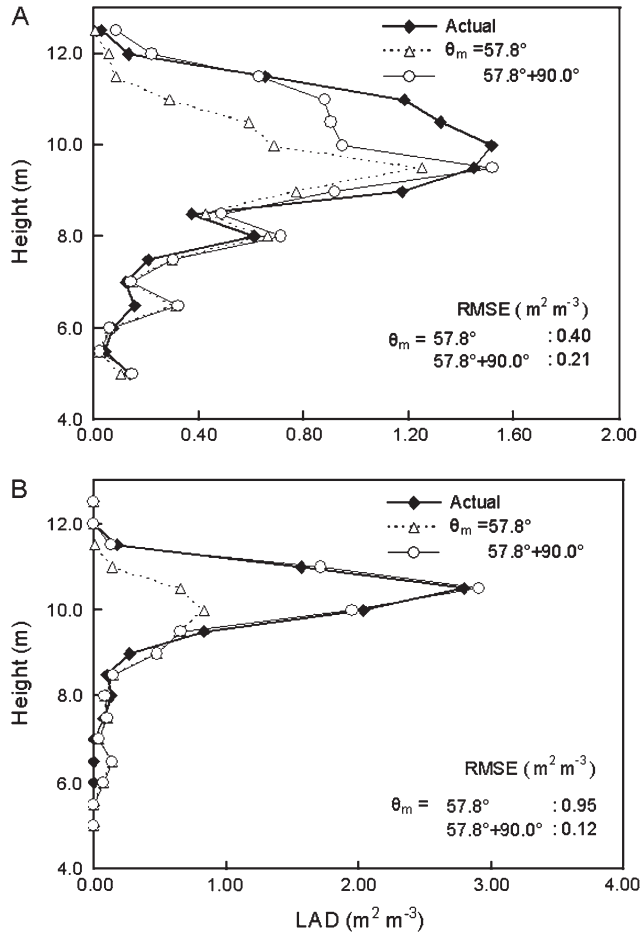

Fig. 6. Comparison of LAD profiles between estimates from the ground measurements and estimates obtained for composite data from measurements from the ground and from a height of 10 m. Open triangle, profile from the six ground measurements at a measurement zenith angle (θ_m) of 57.8 °. Open circle, profile obtained with a composite of the LAD estimates from the ground measurements at a θ_m of 57.8 ° and one from three measurements at a height of 10 m. (A) The measurement plot. (B) Quadrat 2-3. RMSE, root-mean-square error of the LAD estimates.

The relationships in Fig. 7 were fitted well using a power function:

$$\mathrm{RMSE} = aN^b \qquad (5)$$

This function is characterized by the coefficient a and the scaling exponent b. Figure 7 indicates that a increased and b decreased as the measurement zenith angle increased.

It was hypothesized that the change in a and b for each measurement zenith angle relates to the change in $G(\theta_m)$ that accompanies the increase in the measurement zenith angle, and $G(\theta_m)$ was calculated for each measurement zenith angle and the result related to the corresponding values of a and b. As shown in Fig. 8A for coefficient a and Fig. 8B for the scaling exponent b, the resulting relationships could be expressed as functions of $G(\theta_m)$ as follows:

$$a = -22.48 \ln[G(\theta m)] - 5.808 \; R^2 = 0.992 \qquad (6)$$

$$b = 0.183 \ln[G(\theta_m)] - 0.171 \; R^2 = 0.999 \qquad (7)$$

From Equations (5) to (7), the RMSE at each angle was expressed as a common function of N and $G(\theta_m)$.

Discussion

As reported in previous studies (Radtke and Bolstad, 2001; Henning and Radtke, 2006; Hosoi and Omasa, 2006), the presence of non-photosynthetic tissues and the distribution of leaf inclination angles were responsible for estimation errors. The influences of non-photosynthetic tissues in measurements taken from the ground increased as the measurement zenith angle increased because the trunks and branches of the zelkova canopy stretched more vertically than the leaves. The laser beam directions became approximately perpendicular to the trunks and branches, and parallel to the leaves as the measurement angle increased, so that the ratio of the number of incidences of the laser striking trunks and branches to the incidences striking the leaves would have increased as the angle increased. A similar effect that is observed in the gap fraction method was discussed by Chen and Black (1991), who defined $G(\theta)$ based on the inclination angles of both the leaves and the branches. The relatively small effect at a measurement angle of 90.0° in the measurements at a height of 10 m would result from fewer laser beams striking the trunks and branches in the inner canopy due to obstruction by the dense leaves at this height.

Measurements in the leafless condition permitted separation of 3D portable lidar data into leaves and non-photosynthetic tissues. As described above, the ratio of the number of points corresponding to non-photosynthetic tissues within the leafy image was different in each of the measurement angles, but the difference did not affect the effectiveness of the separation because the image taken during the leafless season included almost all parts of non-photosynthetic tissues and the separation was done by extracting corresponding points between the leafless and leafy images based on the voxel coordinates. Besides this method, processing the lidar data with additional information about trees, such as difference in colour, reflectance, and texture in each of the tree tissues, may also be a possible way of achieving the separation.

A laser zenith angle of around 57.5° permitted effective correction for leaf inclination without angle measurements for the woody canopy as well for as individual trees (Hosoi and Omasa, 2006; Omasa *et al.*, 2007). Another way to correct for leaf inclination, using the mean value of $\cos(\theta_{lmn})[G(\theta_{lmn})]^{-1}$ calculated from the lidar-derived distribution of leaf inclination angles, would perform

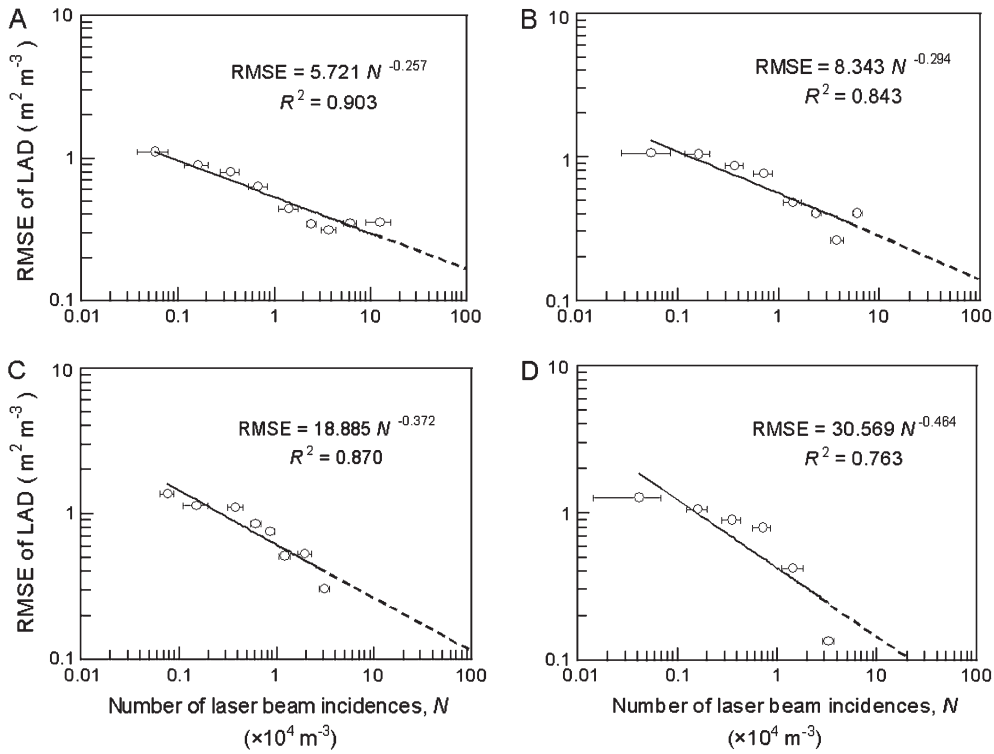

Fig. 7. Relationships between the root-mean-square error (RMSE) of the LAD estimates and the number of laser beam incidences in each cell (*N*). The measurement zenith angles are (A) 47.2 °, (B) 57.8 °, (C) 71.3 °, and (D) 90.0 °. Error bars are standard deviations.

effectively where the 57.5° angle cannot be used due to physical restrictions on the allowable angle. The correction on the lidar-derived leaf inclination angle distribution will be particularly useful at the measurement zenith angle around 90.0°, where the measurement is strongly affected by leaf inclination.

An error in the LAD estimations (Figs 4, 5) was caused despite the above-mentioned corrections. This error depends on the number of incident laser beams within each cell (*N*) at each angle (Fig. 7). In measurements from the ground, the distance between the canopy and the lidar increased as the zenith angle increased, while the increments in the azimuth and zenith angles remained constant at 0.054°. Thus, the values of *N* decreased as the zenith angle increased, and LAD estimates would become more accurate at smaller zenith angles (Figs 4, 5). However, the 90.0° angle at a height of 10 m was the exception. Although the mean value of *N* was smallest at a measurement zenith angle of 90.0° due to the decreased number of measurement positions, the LAD estimate offered the best results of all measurement zenith angles. The exception at 90.0° suggests the presence of another factor that affects the accuracy of LAD estimation.

One possible factor that could explain this result is the difference in the quantity of obstructed leaves at each measurement zenith angle. In this context, 'obstructed' refers to leaves that the laser beams cannot reach as a result of obstruction by other leaves. The presence of these leaves causes an error in LAD estimation, and the degree of obstruction would differ among measurement zenith angles. The degree of the obstruction might be assessed by projection of leaf area on a plane perpendicular to the direction of the laser beam. The mean of this projection would be expressed as $G(\theta_m)$; thus the degree of the obstruction should be reflected in $G(\theta_m)$. In the present study, the value of $G(\theta_m)$ decreased as the measurement zenith angle increased; thus it is expected that the obstruction at large measurement angles decreases compared with the value at small zenith angles. This seems to be supported by the results in Fig. 7, in which the 90.0° angle offered better results than the other angles as *N* increases. These considerations are also supported by the results in Fig. 8, in which parameters *a* and *b* (which express the differences among the fitting functions for the measurement angles) were described as functions of $G(\theta_m)$. These fitting functions to provide a relationship between RMSE and *N* were expressed as a function of *N* and $G(\theta_m)$, as presented in Equations (5) to (7).

Based on this discussion, the results demonstrate that the factors that affect the accuracy of LAD estimation using 3D portable lidar imaging were the presence of non-photosynthetic tissues, the distribution of leaf inclination angles, *N*, and $G(\theta_m)$. By considering these factors in the lidar measurements, more accurate LAD estimates can be obtained. In measurements obtained from the ground, a larger zenith angle will provide more accurate results

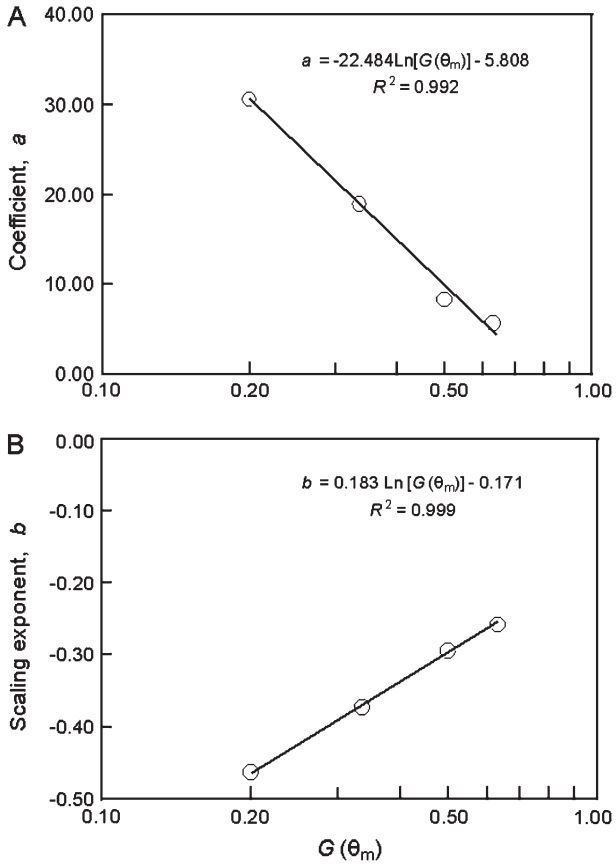

Fig. 8. Relationship between the mean projection of a unit leaf area on a plane perpendicular to the direction of the laser beam at θ_m [$G(\theta_m)$] and the parameters a and b in Equation (5). (A) $G(\theta_m)$ versus coefficient a. (B) $G(\theta_m)$ versus scaling exponent b. θ_m represents the measurement zenith angle.

when a sufficiently high N can be provided by means of fine increments of the laser scan angles from several measurement positions and when the distribution of leaf inclination angles can be measured. A measurement zenith angle of around 57.5° would be useful when it is not possible to measure the distribution of leaf inclination angles. If appropriate measurement positions are available, measurements from higher positions would allow more direct scanning of the dense upper canopy by a sufficient number of laser beams and would thus give a more accurate estimate. Compositing ground-based measurements and measurements taken from a position higher above the ground would provide better estimates in the presence of blind regions both from the ground and from higher positions. These various strategies for improving 3D portable lidar imaging for LAD estimation would also apply to the estimation of LAI, which represents the vertical integration of LAD. However, care should be taken to ensure that the over- and underestimations of LAD will cancel each other out in order to reduce the error in the LAI estimate. The factors affecting LAD estimation error with 3D portable lidar imaging demonstrated in this study would be common to other broadleaved canopies, and the methods used in this study seem to be applicable to them. In coniferous canopies, they have different structure from broadleaved ones and thus additional work would be needed.

References

Anisimov O, Fukshansky L. 1993. Light–vegetation interaction: a new stochastic approach for description and classification. *Agricultural and Forest Meteorology* **66,** 93–110.

Besl PJ, McKay ND. 1992. A method for registration of 3-D shapes. *IEEE Transactions on Pattern Analysis and Machine Intelligence* **14,** 239–256.

Brandtberg T, Warner TA, Landenberger RE, McGraw JB. 2003. Detection and analysis of individual leaf-off tree crowns in small footprint, high sampling density lidar data from the eastern deciduous forest in North America. *Remote Sensing of Environment* **85,** 290–303.

Bréda NJJ. 2003. Ground-based measurements of leaf area index: a review of methods, instruments and current controversies. *Journal of Experimental Botany* **54,** 2403–2417.

Chason JW, Baldocchi DD, Huston MA. 1991. A comparison of direct and indirect methods for estimating forest canopy leaf area. *Agricultural and Forest Meteorology* **57,** 107–128.

Chen JM, Black TA. 1991. Measuring leaf area index of plant canopies with branch architecture. *Agricultural and Forest Meteorology* **57,** 1–12.

Chen JM, Cihlar J. 1995. Plant canopy gap-size analysis theory for improving optical measurements of leaf-area index. *Applied Optics* **34,** 6211–6222.

Ehleringer JR, Field CB. 1993. *Scaling physiological processes—leaf to globe*. San Diego: Academic Press.

Eschenbach C, Kappen L. 1996. Leaf area index determination in an alder forest: a comparison of three methods. *Journal of Experimental Botany* **47,** 1457–1462.

Gower ST, Norman JM. 1991. Rapid estimation of leaf area index in conifer and broad-leaf plantations. *Ecology* **72,** 1896–1900.

Graetz RD. 1990. Remote sensing of terrestrial ecosystem structure: an ecologist's pragmatic view. In: Hobbs RJ, Mooney HA, eds. *Remote sensing of biosphere functioning*. New York: Springer, 5–30.

Groeneveld DP. 1997. Vertical point quadrat sampling and an extinction factor to calculate leaf area index. *Journal of Arid Environments* **36,** 475–485.

Harding DJ, Lefsky MA, Parker GG, Blair JB. 2001. Laser altimeter canopy height profiles. Methods and validation for closed-canopy, broadleaf forests. *Remote Sensing of Environment* **76,** 283–297.

Henning JG, Radtke PJ. 2006. Ground-based laser imaging for assessing three-dimensional forest canopy structure. *Photogrammetric Engineering and Remote Sensing* **72,** 1349–1358.

Holmgren J, Persson Å. 2004. Identifying species of individual trees using airborne laser scanner. *Remote Sensing of Environment* **90,** 415–423.

Hosoi F, Omasa K. 2006. Voxel-based 3-D modeling of individual trees for estimating leaf area density using high-resolution portable scanning lidar. *IEEE Transactions on Geoscience and Remote Sensing* **44,** 3610–3618.

Hosoi F, Yoshimi K, Shimizu Y, Omasa K. 2005. 3-D measurement of trees using a portable scanning lidar. *Phyton – Annals Rei Botanicae* **45,** 497–500.

Houldcroft CJ, Campbell CL, Davenport IJ, Gurney RJ, Holden N. 2005. Measurement of canopy geometry characteristics

using LiDAR laser altimetry: a feasibility study. *IEEE Transactions on Geoscience and Remote Sensing* **43,** 2270–2282.

Hyyppä J, Inkinen M. 1999. Detecting and estimating attributes for single trees using laser scanner. *Photogrammetric Journal of Finland* **16,** 27–42.

Hyyppä J, Kelle O, Lehikoinen M, Inkinen M. 2001. A segmentation-based method to retrieve stem volume estimates from 3-D tree height models produced by laser scanners. *IEEE Transactions on Geoscience and Remote Sensing* **39,** 969–975.

Jonckheere I, Fleck S, Nackaerts K, Muys B, Coppin P, Weiss M, Baret F. 2004. Review of methods for *in situ* leaf area index determination. Part I. Theories, sensors and hemispherical photography. *Agricultural and Forest Meteorology* **121,** 19–35.

Jones HG. 1992. *Plants and microclimate*, 2nd edn. Cambridge: Cambridge University Press.

Jones HG, Archer N, Rotenberg E, Casa R. 2003. Radiation measurement for plant ecophysiology. *Journal of Experimental Botany* **54,** 879–889.

Lang ARG, Yueqin X. 1986. Estimation of leaf area index from transmission of direct sunlight in discontinuous canopies. *Agricultural and Forest Meteorology* **37,** 229–243.

Larcher W. 2001. *Physiological plant ecology*, 4th edn. Heidelberg: Springer.

Leblanc SG, Chen JM, Fernandes R, Deering DW, Conley A. 2005. Methodology comparison for canopy structure parameters extraction from digital hemispherical photography in boreal forests. *Agricultural and Forest Meteorology* **129,** 187–207.

Lefsky MA, Cohen WB, Parker GG, Harding DJ. 2002. Lidar remote sensing for ecosystem studies. *Bioscience* **52,** 19–30.

Lovell JL, Jupp DLB, Culvenor DS, Coops NC. 2003. Using airborne and ground-based ranging lidar to measure canopy structure in Australian forests. *Canadian Journal of Remote Sensing* **29,** 607–622.

MacArthur RH, Horn HS. 1969. Foliage profile by vertical measurements. *Ecology* **50,** 802–804.

Magnussen S, Boudewyn P. 1998. Derivations of stand heights from airborne laser scanner data with canopy-based quantile estimators. *Canadian Journal of Forest Research* **28,** 1016–1031.

Monteith JL. 1973. *Principles of environmental physics*. London: Edward Arnold.

Morsdorf F, Kötz B, Meier E, Itten KI, Allgöwer B. 2006. Estimation of LAI and fractional cover from small footprint airborne laser scanning data based on gap fraction. *Remote Sensing of Environment* **104,** 50–61.

Næsset E, Gobakken T, Holmgren J, Hyyppä H, Hyyppä J, Maltamo M, Nilsson M, Olsson H, Persson Å, Söderman U. 2004. Laser scanning of forest resources: the Nordic experience. *Scandinavian Journal of Forest Research* **19,** 482–499.

Neumann HH, Hartog GD, Shaw RH. 1989. Leaf area measurements based on hemispheric photographs and leaf-litter collection in a deciduous forest during autumn leaf-fall. *Agricultural and Forest Meteorology* **45,** 325–345.

Norman JM, Campbell GS. 1989. Canopy structure. In: Pearcy RW, Ehleringer J, Mooney HA, Rundel PW, eds. *Plant physiological ecology: field methods and instrumentation*. London: Chapman and Hall, 301–325.

Omasa K, Akiyama Y, Ishigami Y, Yoshimi K. 2000. 3-D remote sensing of woody canopy heights using a scanning helicopter-borne lidar system with high spatial resolution. *Journal of Remote Sensing Society of Japan* **20,** 394–406.

Omasa K, Hosoi F, Konishi A. 2007. 3D lidar imaging for detecting and understanding plant responses and canopy structure. *Journal of Experimental Botany* **58,** 881–898.

Omasa K, Qiu GY, Watanuki K, Yoshimi K, Akiyama Y. 2003. Accurate estimation of forest carbon stocks by 3-D remote sensing of individual trees. *Environmental Science and Technology* **37,** 1198–1201.

Omasa K, Urano Y, Oguma H, Fujinuma Y. 2002. Mapping of tree position of *Larix leptolepis* woods and estimation of diameter at breast height (DBH) and biomass of the trees using range data measured by a portable scanning lidar. *Journal of Remote Sensing Society of Japan* **22,** 550–557.

Parker GG, Harding DJ, Berger ML. 2004. A portable LIDAR system for rapid determination of forest canopy structure. *Journal of Applied Ecology* **41,** 755–767.

Radtke PJ, Bolstad PV. 2001. Laser point-quadrat sampling for estimating foliage-height profiles in broad-leaved forests. *Canadian Journal of Forest Research* **31,** 410–418.

Riaño D, Meier E, Allgöwer B, Chuvieco E, Ustin SL. 2003. Modeling airborne laser scanning data for the spatial generation of critical forest parameters in fire behavior modeling. *Remote Sensing of Environment* **86,** 177–186.

Ross J. 1981. *The radiation regime and architecture of plant stands*. The Hague: The Netherlands Dr W. Junk.

Schurr U, Walter A, Rascher U. 2006. Functional dynamics of plant growth and photosynthesis——from steady-state to dynamics—from homogeneity to heterogeneity. *Plant, Cell and Environment* **29,** 340–352.

Solberg S, Næsset E, Hanssen KH, Christiansen E. 2006. Mapping defoliation during a severe insect attack on Scots pine using airborne laser scanning. *Remote Sensing of Environment* **102,** 364–376.

Stokes VJ, Morecroft MD, Morison JIL. 2006. Boundary layer conductance for contrasting leaf shapes in a deciduous broadleaved forest canopy. *Agricultural and Forest Meteorology* **139,** 40–54.

Takeda T, Oguma H, Yone Y, Yamagata Y, Fujinuma Y. 2005. Comparison of leaf area density measured by laser range finder and stratified clipping method. *Phyton – Annals Rei Botanicae* **45,** 505–510.

Tanaka T, Park H, Hattori S. 2004. Measurement of forest canopy structure by a laser plane range-finding method. Improvement of radiative resolution and examples of its application. *Agricultural and Forest Meteorology* **125,** 129–142.

Vanderbilt VC, Silva LF, Bauer ME. 1990. Canopy architecture measured with a laser. *Applied Optics* **29,** 99–106.

Warren-Wilson J. 1960. Inclined point quadrats. *New Phytologist* **59,** 1–8.

Warren-Wilson J. 1963. Estimation of foliage denseness and foliage angle by inclined point quadrats. *Australian Journal of Botany* **11,** 95–105.

Weiss M, Baret F, Smith GJ, Jonckheere I, Coppin P. 2004. Review of methods for *in situ* leaf area index (LAI) determination. Part II. Estimation of LAI, errors and sampling. *Agricultural and Forest Meteorology* **121,** 37–53.

Welles JM, Cohen S. 1996. Canopy structure measurement by gap fraction analysis using commercial instrumentation. *Journal of Experimental Botany* **47,** 1335–1342.

Welles JM, Norman JM. 1991. Instrument for indirect measurement of canopy architecture. *Agronomy Journal* **83,** 818–825.

Yoshimi K, Hosoi F, Shimizu Y, Yamada H, Omasa K. 2004. 3-D measurement of terrain and woody canopy height using portable scanning lidar. *Eco-Engineering* **16,** 203–207.

Yu X, Hyyppä J, Kaartinen H, Maltamo M. 2004. Automatic detection of harvested trees and determination of forest growth using airborne laser scanning. *Remote Sensing of Environment* **90,** 451–462.